journal

J. Am. Ceram. Soc., 98 [6] 1870–1876 (2015)
DOI: 10.1111/jace.13553

Synthesis, Crystal Structure, and Enhanced Luminescence of Garnet-Type $Ca_3Ga_2Ge_3O_{12}$:Cr^{3+} by Codoping Bi^{3+}

Chengyin Liu,[‡,§] Zhiguo Xia,[‡,†] Maxim S. Molokeev,[¶] and Quanlin Liu[‡]

[‡]School of Materials Sciences and Engineering, University of Science and Technology Beijing, Beijing 100083, China

[§]School of Materials Sciences and Technology, China University of Geosciences, Beijing 100083, China

[¶]Laboratory of Crystal Physics, Kirensky Institute of Physics, SB RAS, Krasnoyarsk 660036, Russia

Garnet-type compound $Ca_3Ga_2Ge_3O_{12}$ and Cr^{3+}-doped or Cr^{3+}/Bi^{3+} codped $Ca_3Ga_2Ge_3O_{12}$ phosphors were prepared by a solid-state reaction. The crystal structure of $Ca_3Ga_2Ge_3O_{12}$ host was studied by X-ray diffraction (XRD) analysis and further determined by the Rietveld refinement. Near-infrared (NIR) photoluminescence (PL) and long-lasting phosphorescence (LLP) emission can be observed from the Cr^{3+}-doped $Ca_3Ga_2Ge_3O_{12}$ sample, and the enhanced NIR PL emission intensity and LLP decay time can be realized in Cr^{3+}/Bi^{3+} codped samples. The optimum concentration of Cr^{3+} in $Ca_3Ga_2Ge_3O_{12}$ phosphor was about 6 mol%, and optimum Bi^{3+} concentration induced the energy-transfer (ET) process between Bi^{3+} and Cr^{3+} ions was about 30 mol%. Under different excitation wavelength from 280 to 453 nm, all the samples exhibit a broadband emission peaking at 739 nm and the intensity of NIR emission increases owing to the ET behavior from Bi^{3+} to Cr^{3+} ions. The critical ET distance has been calculated by the concentration-quenching method. The thermally stable luminescence properties were also studied and the introduction of Bi^{3+} can also improve the thermal stability of the NIR emission.

I. Introduction

Inorganic phosphors showing near-infrared (NIR) luminescence have been rapidly developed in recent years owing to their promising feature from security signs to *in vivo* imaging systems.[1,2] For examples, this kind of phosphor showing NIR emission demonstrates advantages in the spectral conversion as high efficient luminescent solar concentrator and high signal-to-noise ratio for optical detecting application. Moreover, the NIR emission belongs to the non-invasive visualization tools, which can offer great advantages in terms of cost and simplicity over other traditional optical imaging systems.[2] Among all the reported NIR emission materials, chromium ion (Cr^{3+}) has been reported to be a kind of favorable luminescent center, which was ascribed to the emissions around 700 nm due to the $^4E \rightarrow {}^4A_2$ transition, so that the broad and intense emission bands in the red and the near infrared associated with *d–d* electronic transitions of octahedral Cr^{3+} ions have been intensively investigated. Cr^{3+}-doped NIR luminescence materials can be found from the references, such as $Zn_3Ga_2Ge_2O_{10}$:Cr^{3+},[3] Zn$(Ga_{1-x}Al_x)_2O_4$:Cr^{3+},Bi^{3+},[4] $ZnGa_2O_4$:Cr^{3+},[5] $La_3Ga_5GeO_{14}$:Cr^{3+},[6] $LiGa_5O_8$:Cr^{3+}[7], and some potential applications including the NIR long-lasting phosphorescence (LLP) emitters, *in vivo* bioimaging or advanced optical devices have been also reported.[8,9] In general, Cr^{3+} ions will substitute for Ga^{3+} ions in GaO_6 octahedral sites and the phosphors exhibit NIR luminescence. Accordingly, we can explore some possible hosts containing the GaO_6 octahedral sites, which in turn can generate NIR luminescence when it is doped by Cr^{3+}.

Garnet-type $X_3Y_2(TO_4)_3$ host representing by $Y_3Al_3O_{12}$ and $Ca_3Sc_2Si_3O_{12}$ can act as the excellent white light LEDs phosphor after Ce^{3+} doping.[10,11] It is well-known that garnet phosphors are unique in their tunability of the luminescence properties through variations in the {X}, [Y], and (T) cation sublattice. The X site can be replaced by the rare earth ions, such as Y^{3+}, Lu^{3+}, Gd^{3+}, Tb^{3+} or La^{3+} ions, or divalent cations, such as Ca^{2+}, Mn^{2+}; and Y site can be replaced by Al^{3+}, Ga^{3+}, Sc^{3+} or by Sb^{3+}, In^{3+}, even the Mg^{2+}. T site can also be replaced by Al^{3+}, or Si^{4+} or Ge^{4+} while maintaining the garnet crystal structure type. Therefore, the very wide solid solution compositional variation enables optimization of properties, and excellent photoluminescence properties may be expected in such a system when the suitable activator ions were introduced. Here, the $Ca_3Ga_2Ge_3O_{12}$ host was proposed and some interesting luminescence properties have been studied in such a phosphor system. Very recently, Chen *et al.* also reported the Cr/Yb/Tm:$Ca_3Ga_2Ge_3O_{12}$ phosphor, which exhibits both broadband NIR LLP of Cr^{3+} and NIR to NIR upconversion luminescence of Tm^{3+}.[12]

Our present studies have paid more attention to the crystal structure understanding of $Ca_3Ga_2Ge_3O_{12}$ and the modification of the NIR photoluminescence (PL), also including the LLP emission based on the composition regulation and codoping effect of Bi^{3+} and Cr^{3+} ions. In general, novel phosphor materials showing NIR light need a suitable emitter, such as Cr^{3+}, however, the LLP luminescence require a proper host which is able to create appropriate traps. Therefore, the effects of Cr^{3+}/Bi^{3+} codoped behavior in $Ca_3Ga_2Ge_3O_{12}$ on the PL and LLP luminescence properties were discussed in this study, and the luminescence and energy-transfer mechanism have been investigated in detail.

II. Experimental Procedure

(1) Materials and Synthesis

$Ca_3Ga_2Ge_3O_{12}$:Cr^{3+}, $Ca_3Ga_2Ge_3O_{12}$:Bi^{3+}, and $Ca_3Ga_2Ge_3O_{12}$:Cr^{3+},Bi^{3+} phosphors were synthesized by a solid-state reaction method using $CaCO_3$ (99.9%), Ga_2O_3 (99.9%), GeO_2 (99.9%), Cr_2O_3 (99.9%), and Bi_2O_3 (99.9%) as starting materials, in which 5 mol% of Li_2CO_3(99.9%) was used as a flux, and the nominal chemical compositions for the phosphors can be designed as $Ca_3Ga_{2-x-y}Ge_3O_{12}$:xCr^{3+}, yBi^{3+}. Therefore, the starting materials were weighed stoichiometrically and finely mixed in an agate mortar to ensure homogeneous mixing. Then the mixed samples were fired in air at 1000°C for

H. Guo—contributing editor

Manuscript No. 36034. Received December 8, 2014; approved February 12, 2015.
†Author to whom correspondence should be addressed. e-mail: xiazg@ustb.edu.cn

3 h. After that, the samples were furnace-cooled to room temperature and finely ground to obtain the final products.

(2) Characterization Methods

X-ray diffraction (XRD) patterns were performed using SHIMADZU (Kyoto, Japan) model XRD-6000 diffractometer with CuK_α radiation (λ = 0.15406 nm) at 40 kV, 30 mA, and the data were collected between 10° and 70°. The data for Rietveld analysis were collected between 10° and 120° with the same diffractometer, and the step size of 2θ was 0.016°, and the counting time was 1 s per step. Rietveld refinement was performed using TOPAS 4.2.[13] Photoluminescence excitation (PLE), PL, and LLP spectra were recorded on a F4600 fluorescence spectrophotometer (HITACHI, Tokyo, Japan) with a photomultiplier tube operating at 400 V, and a 150 W Xe lamp used as the excitation lamp. The temperature-dependent luminescence properties were measured on the same spectrophotometer, which was equipped with a home-made computer-controlled electric furnace. The decay curves were recorded on a spectrophotometer (HORIBA, JOBIN YVON FL3-21, Paris, France), and the 465 nm pulse laser radiation attachment (spectral-LED for the microsecond lifetime measurement) was used as the excitation source.

III. Results and Discussion

(1) Phase Structure of the Samples

The powder diffraction data of as-prepared $Ca_3Ga_2Ge_3O_{12}$ host powder was firstly analyzed via the Rietveld refinement. Almost all peaks were indexed by cubic cell (*Ia*-3*d*) with parameters close to $Ca_3Fe_2Ge_3O_{12}$ (garnet-type structure). Therefore, crystal structure of $Ca_3Fe_2Ge_3O_{12}$ was taken as a starting model for Rietveld refinement. Site of Fe ion was occupied by Ga ion. Refinement was stable and gives low *R*-factors (R_B = 1.40%, χ^2 = 3.78), and the refined pattern was shown in Fig. 1. However, it was also found that there was a diffraction peak around 30.5° originating from the remaining starting material Ga_2O_3, but it would not affect the phase determination of the $Ca_3Ga_2Ge_3O_{12}$. The crystal structure is cubic (space group *Ia*-3*d*) with lattice constants *a* = 12.2562 (1) Å, *V* = 1841.05 (5) Å^3, and *Z* = 2, as shown in Table I. The crystallographic information file of the present $Ca_3Ga_2Ge_3O_{12}$ compound via the Rietveld refinement was also presented in attached supplementary information. Moreover, the inset of Fig. 1 represents the crystal structure of the $Ca_3Ga_2Ge_3O_{12}$ host, which belongs to the cubic garnet-type $A_3B_2C_3X_{12}$ structure mentioned above. In this structure, each [GaO_6] octahedron is connected with six [GeO_4] tetrahedrons, each [GeO_4] tetrahedron is connected with four [GaO_6] octahedrons, and the octahedrons and tetrahedrons are linked by corner-sharing, which results in the formation of the dodecahedron void. Therefore, the Ca^{2+} cations occupy the center of the dodecahedron void.[12]

Table I. Main Parameters of Processing and Refinement of the $Ca_3Ga_2Ge_3O_{12}$ Sample

Compound	$Ca_3Ga_2Ge_3O_{12}$
Sp.Gr.	*Ia*-3*d*
a, Å	12.2562 (1)
V, Å^3	1841.05 (5)
Z	2
2θ-interval, °	12–120
Number of reflections	117
Number of parameters of refinement	43
R_{wp}, %	11.28
R_p, %	7.73
R_{exp}, %	2.98
χ^2	3.78
R_B, %	1.40

The phase structure of the as-synthesized $Ca_3Ga_2Ge_3O_{12}$ sample and Cr^{3+} singly doped or Cr^{3+}/Bi^{3+} codoped $Ca_3Ga_2Ge_3O_{12}$ samples were further studied by the powder X-ray diffraction. Figure 2 shows the XRD patterns of as-prepared $Ca_3Ga_2Ge_3O_{12}$ host powder, $Ca_3Ga_{1.94}Ge_3O_{12}$:0.06Cr^{3+}, $Ca_3Ga_{1.64}Ge_3O_{12}$:0.06Cr^{3+},0.3Bi^{3+}, $Ca_3Ga_{1.44}Ge_3O_{12}$:0.06Cr^{3+},0.5Bi^{3+}, and $Ca_3Ga_{1.14}Ge_3O_{12}$:0.06Cr^{3+}, 0.8Bi^{3+} phosphors, the standard file of JCPDS card (11-0023) of $Ca_3Ga_2Ge_3O_{12}$ phase was also given as a reference. After a careful comparison, it is found that the relative intensities and peak positions of as-prepared powder samples agree well with the standard data for $Ca_3Ga_2Ge_3O_{12}$ when the doping amount of Bi^{3+} was below 0.3 although there are some minor peaks belonging to the $CaGa_2O_4$ by-product, which cannot affect the doping effect of Cr^{3+} and/or Bi^{3+} ions. However, some impurities originating from $Bi_4(GeO_4)_3$ can be clearly found from the diffraction patterns for the as-prepared samples when the Bi^{3+} contents were corresponding to 0.5 and 0.8, which indicated that Bi^{3+} can be partly dissolved in the garnet-type $Ca_3Ga_2Ge_3O_{12}$ host. Nevertheless, the amount of the impurities is minor and it cannot affect the luminescence properties obviously.

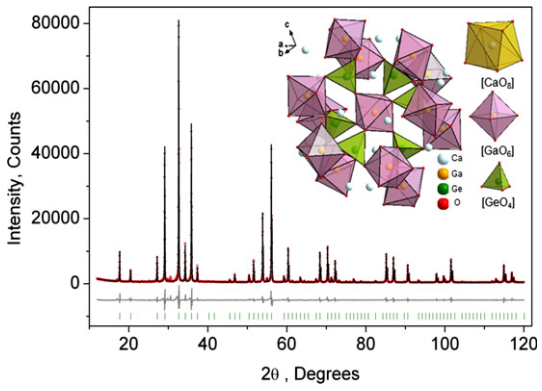

Fig. 1. Rietveld analysis patterns for X-ray powder diffraction data of the as-prepared $Ca_3Ga_2Ge_3O_{12}$ compound. The solid black lines are calculated intensities, and the red dots are the observed intensities. The gray solid lines below the profiles stand for the difference between the observed and calculated intensities. The short green vertical lines show the position of Bragg reflections of the calculated pattern. The inset shows the schematic diagram of $Ca_3Ga_2Ge_3O_{12}$ structure and coordination environment of the Ca^{2+}, Ga^{3+}, and Ge^{4+} cations.

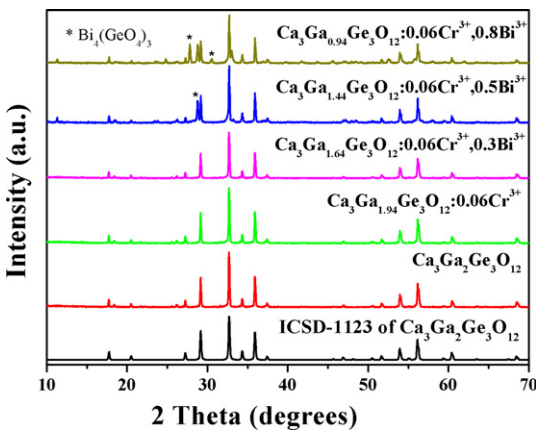

Fig. 2. XRD patterns of as-prepared $Ca_3Ga_2Ge_3O_{12}$ host, $Ca_3Ga_{1.94}Ge_3O_{12}$:0.06Cr^{3+}, $Ca_3Ga_{1.64}Ge_3O_{12}$:0.06Cr^{3+},0.3Bi^{3+}, $Ca_3Ga_{1.44}Ge_3O_{12}$:0.06Cr^{3+},0.5Bi^{3+} and $Ca_3Ga_{1.14}Ge_3O_{12}$:0.06Cr^{3+},0.8Bi^{3+} phosphors, and the standard data for $Ca_3Ga_2Ge_3O_{12}$ compound as reference.

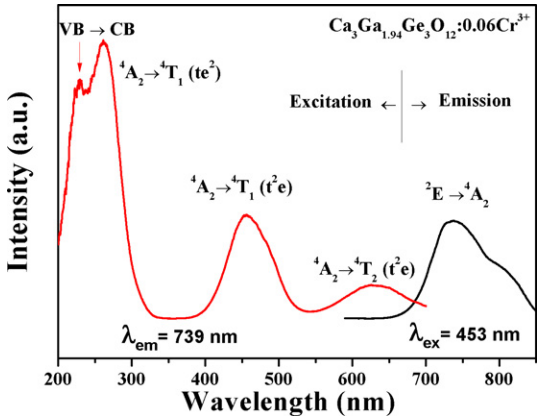

Fig. 3. Photoluminescence excitation and emission spectra of as-prepared $Ca_3Ga_{1.94}Ge_3O_{12}$:0.06Cr^{3+} phosphor. The emission spectrum is acquired under 453 nm light excitation and the excitation spectrum is obtained by monitoring 739 nm emission.

(2) Luminescence and Properties of the Samples

Figure 3 shows the PLE and emission (PL) spectra of typical $Ca_3Ga_{1.94}Ge_3O_{12}$:0.06Cr^{3+} phosphor. Under excitation at 453 nm, the sample exhibits a broadening $^2E \rightarrow ^4A_2$ emission peaking at 739 nm that superimposes on a broad background emission ranging from ~600 to ~850 nm. The broadening of the $^2E \rightarrow ^4A_2$ emission is possibly caused by the electron-phonon coupling in the host system. The PLE spectrum monitored at 739 nm covers a very broad spectral region (from 200 to 700 nm) and consists of three main excitation bands originating from the *d*–*d* inner transitions of Cr^{3+}, including the 261 nm band originating from the $^4A_2 \rightarrow ^4T_1$ (te^2) transition, the 452 nm band originating from the $^4A_2 \rightarrow ^4T_1$ (t^2e) transition and the 625 nm band originating from the $^4A_2 \rightarrow ^4T_2$(t^2e) transition.[14,15] In addition, band gap transition (VB→CB) at around 228 nm was also detected from the PLE spectrum. Furthermore, a schematic diagram of the related energy levels for $Ca_3Ga_2Ge_3O_{12}$:Cr^{3+} phosphors is depicted in Fig. 4. As for the photoluminescence process, under light excitation corresponding to different wavelength, such as 261 nm, the ground-state electrons of Cr^{3+} ions are promoted to the $^4T_1$ (te^2) level. The excited electrons will relax to the ^2E energy level, and show the NIR emission via the $^2E \rightarrow ^4A_2$ transition. Moreover, the NIR LLP emission can be also observed in such a system. In this case, the excited electrons are partly captured by electron traps. After a suitable illumination time, those traps can store the excited electrons. In general, the sample was firstly irradiated by the 254 nm ultraviolet light for 15 min before the LLP measurement. After the stoppage of the irradiation,

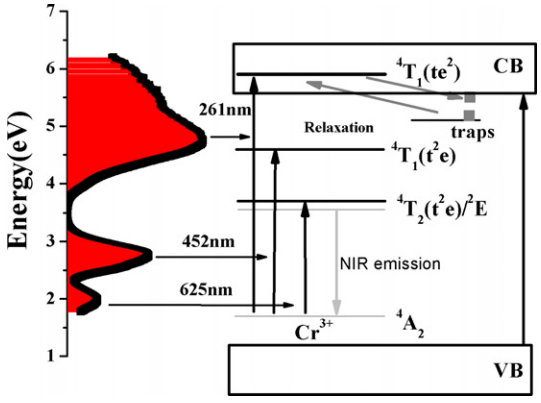

Fig. 4. A schematic diagram of the photoluminescence and long-lasting phosphorescence showing the excitation, electron transitions of Cr^{3+}, and electron traps in $Ca_3Ga_2Ge_3O_{12}$:Cr^{3+} phosphor.

the electrons were released from traps and the ionized Cr^{3+} ions dominate the persistent luminescence process and give the NIR afterglow luminescence. Figure 5(a) gives the afterglow spectrum of the selected $Ca_3Ga_{1.94}Ge_3O_{12}$:0.06Cr^{3+} phosphor acquired after the removal of excitation source with delay time of 20 s. The LLP spectrum exhibited the similar spectral profile as the PL spectrum with a broadband (in the wavelength range 650–850 nm) peaking at near 730 nm, corresponding to the broadening $^2E \rightarrow ^4A_2$ transition of Cr^{3+}. As a comparison, Fig. 5(a) also demonstrates the afterglow spectrum of $Ca_3Ga_{1.64}Ge_3O_{12}$:0.06Cr^{3+},0.3Bi^{3+} samples obtained at the same condition. The same spectral profile can be found except for the low LLP intensities. Figure 5(b) shows the LLP decay curve of the selected $Ca_3Ga_{1.94}Ge_3O_{12}$:0.06Cr^{3+} and $Ca_3Ga_{1.64}Ge_3O_{12}$:0.06Cr^{3+}, 0.3Bi^{3+} phosphor after irradiation by the 254 nm ultraviolet light for 15 min. As shown in Fig. 5(b), the afterglow intensity of the two samples decreases quickly at first and then very slowly. Therefore, the two decay components can be well fitted to a double-exponential function as

$$I(t) = I_0 + A_1 \exp(-t/\tau_1) + A_2 \exp(-t/\tau_2) \quad (1)$$

where I and I_0 are the luminescence intensity, A_1 and A_2 are constants, t is the time, and t_1 and t_2 are the decay times for the exponential components, respectively. The average lifetime τ^* can be obtained by the formula as follows:

$$\tau^* = (A_1\tau_1^2 + A_2\tau_2^2)/(A_1\tau_1 + A_2\tau_2) \quad (2)$$

On the basis of these fitting results in Eq. (1), we can calculate the average lifetime for the two samples are 105 and 56 s for $Ca_3Ga_{1.64}Ge_3O_{12}$:0.06Cr^{3+},0.3Bi^{3+} and $Ca_3Ga_{1.94}Ge_3O_{12}$:0.06Cr^{3+}, respectively. We can find that the prolonged afterglow time can be realized via the codoped effect of Bi^{3+} although the initial LLP intensity can be only found from the Cr^{3+} singly doped sample. It is believed that the introduction of Bi^{3+} can help to the formation of the electron traps as the Cr^{3+}–Bi^{3+} couple in the system, as reported in other reference.[16] Therefore, $Ca_3Ga_{1.64}Ge_3O_{12}$:0.06Cr^{3+},0.3Bi^{3+} sample possess good LLP property compared to that of the singly Cr^{3+}-doped sample.

Figure 6 shows the Cr^{3+} concentration-dependent PL spectra of $Ca_3Ga_{2-x}Ge_3O_{12}$:xCr^{3+} phosphors under 453 nm light excitation, and their spectra possess the similar spectral profile covering the wavelength region from 650 to 850 nm and show the NIR emission with peak at around 739 nm. Furthermore, the inset shows the variation in the Cr^{3+} concentration-dependent PL intensities, and the optimum doping concentration was found at $x = 0.06$. After that, the PL intensity begins to decline owing to the concentration-quenching behavior of Cr^{3+} ions. Then the sample of $Ca_3Ga_{1.94}Ge_3O_{12}$:0.06Cr^{3+} has been selected and proceed with the following study. To explore the effect of the introduction of Bi^{3+} into the $Ca_3Ga_{1.94}Ge_3O_{12}$:0.06Cr^{3+} phosphor, Fig. 7 comparatively gives the PLE and PL spectra of the selected $Ca_3Ga_{1.94}Ge_3O_{12}$:0.06Cr^{3+}, $Ca_3Ga_{1.7}Ge_3O_{12}$: 0.30Bi^{3+}, and $Ca_3Ga_{1.64}Ge_3O_{12}$:0.06Cr^{3+},0.30Bi^{3+} phosphors. Among them, Fig. 7(a) shows the PLE and PL spectra of Cr^{3+} singly doped $Ca_3Ga_2Ge_3O_{12}$ sample. It is found that the PL spectrum upon the excitation of 280 nm has similar spectral profile as found in Figs. 3 and 6. Figure 7(b) gives the PLE and PL spectra of Bi^{3+} singly doped $Ca_3Ga_2Ge_3O_{12}$ sample. The PLE spectrum monitored at 440 nm shows the excitation band peaking at 284 nm, which is assigned to the $^1S_0$–$^1P_1$ transitions of Bi^{3+}.[17] Under the excitation of 284 nm, the PL spectrum display a broadband from 300 to 650 nm with a maximum at about 440 nm. From Figs. 7(a) and (b), we can see that there is an obvious spectral overlap between the emission band of Bi^{3+} and the excitation band of Cr^{3+}, which indicates the possible resonance type energy transfer from Bi^{3+} to Cr^{3+} in $Ca_3Ga_2Ge_3O_{12}$ host. Figure 7(c) shows the PLE and PL spectra of

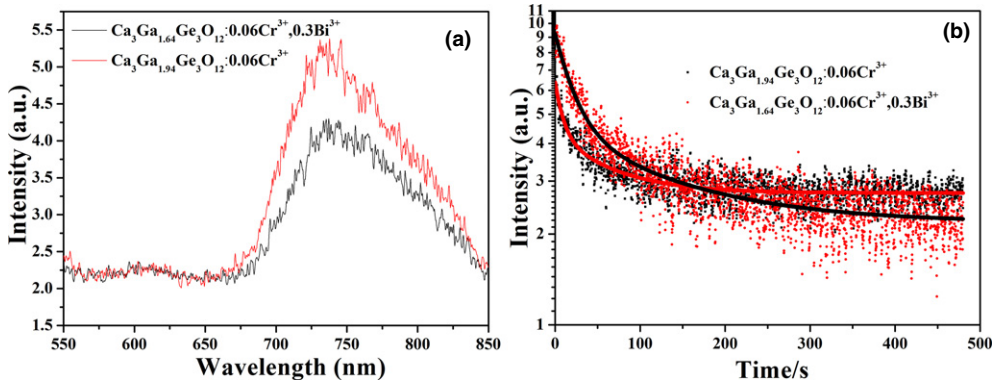

Fig. 5. LLP emission spectra (a) and decay curves (b) of the selected $Ca_3Ga_{1.94}Ge_3O_{12}:0.06Cr^{3+}$ and $Ca_3Ga_{1.64}Ge_3O_{12}:0.06Cr^{3+},0.3Bi^{3+}$ samples.

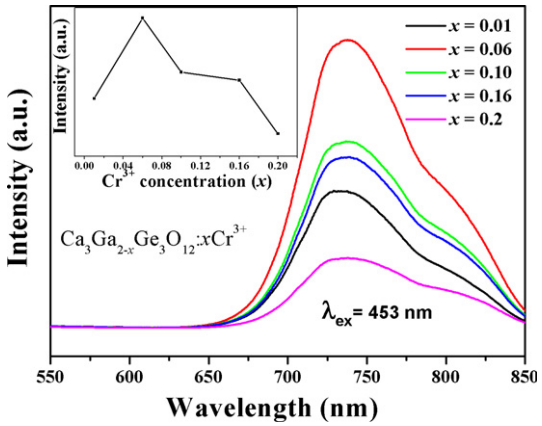

Fig. 6. Cr^{3+} concentration-dependent PL spectra (λ_{ex} = 453 nm) of $Ca_3Ga_2Ge_3O_{12}$: Cr^{3+} phosphors, and the inset shows Cr^{3+} concentration dependence of PL intensity.

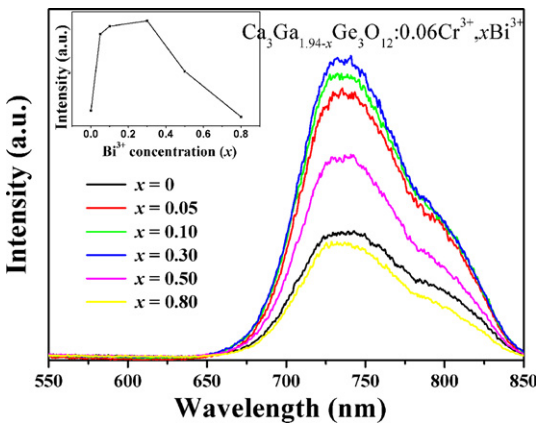

Fig. 8. Bi^{3+} concentration-dependent PL spectra of $Ca_3Ga_{1.94-x}Ge_3O_{12}:0.06Cr^{3+},xBi^{3+}$ samples (λ_{ex} = 453 nm), and the inset shows the Bi^{3+} concentration dependence of PL intensity.

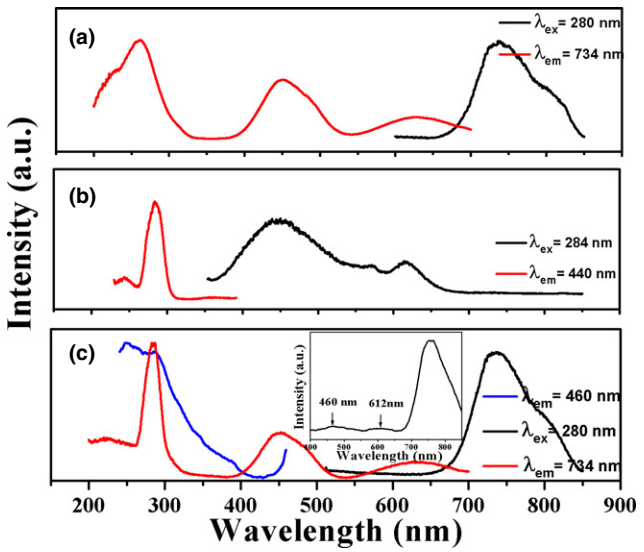

Fig. 7. PLE (left) and PL (right) spectra of $Ca_3Ga_{1.94}Ge_3O_{12}:0.06Cr^{3+}$ (a), $Ca_3Ga_{1.7}Ge_3O_{12}:0.3Bi^{3+}$ (b), and $Ca_3Ga_{1.64}Ge_3O_{12}:0.06Cr^{3+},0.3Bi^{3+}$ (c) samples, and the enlarged PL spectrum of $Ca_3Ga_{1.64}Ge_3O_{12}:0.06Cr^{3+},0.3Bi^{3+}$ in the full range is also given in the inset of (c). The corresponding monitoring wavelengths are also given in the figure.

$Ca_3Ga_{1.64}Ge_3O_{12}:0.06Cr^{3+},0.30Bi^{3+}$ phosphor. We can found that excitation spectrum monitored by 734 nm has similar spectral profile as that of the Bi^{3+} singly doped $Ca_3Ga_2Ge_3O_{12}$ sample, especially the excitation peak at 284 nm. The emission intensity of Cr^{3+} near 734 nm has also been enhanced obviously with the introduction of Bi^{3+} ions owing to the energy-transfer process from Bi^{3+} to Cr^{3+} ions. At the same time, we can also find the typical emission of Bi^{3+} from the enlarged PL spectrum of $Ca_3Ga_{1.64}Ge_3O_{12}:0.06Cr^{3+},0.3Bi^{3+}$ in the full range. Therefore, Fig. 8 exhibits the Bi^{3+} concentration-dependent PL spectra of $Ca_3Ga_{1.94-x}Ge_3O_{12}:0.06Cr^{3+}$, xBi^{3+} samples (λ_{ex} = 453 nm) to find the optimum Bi^{3+} content. With increasing Bi^{3+} concentration, the emission band at 739 nm increases and reaches the maxima at the Bi^{3+} concentration of 0.3, as also shown in the inset of Fig. 8. The main reason for the decrease in the emission intensities should be ascribed to concentration-quenching effect, and energy transfer also happened in such a system. However, it is believed that the impurities can affect the luminescence properties, but it has the minor influence. Therefore, the interaction type between sensitizers or between sensitizer and activator can be calculated by the following equation[18,19]

$$\frac{I}{x} = K\left[1 + \beta(x)^{\frac{\theta}{3}}\right]^{-1} \tag{3}$$

where x is the concentration of the activator ions (Bi^{3+} and Cr^{3+} ions), I is the emission intensity, K and β are constants for the same excitation condition for a given host lattice, and θ is a function of multipole–multipole interaction. When the value of θ is 6, 8, or 10, the interaction types correspond to dipole–dipole (d–d), dipole–quadrupole (d–q), and quadrupole–quadrupole(q–q) interactions, respectively. The dependence of log (I/x) on log (x) was found to be relatively

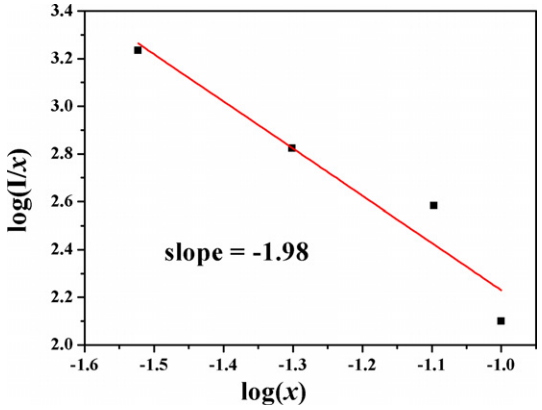

Fig. 9. The fitting line of $\log(I/x)$ vs. $\log(x)$ in $Ca_3Ga_2Ge_3O_{12}$:Cr^{3+} xBi^{3+} phosphors beyond the quenching concentration.

linear, and it yields a straight line with a slope equal to $-\theta/3$, so we can obtain the θ value to study the energy-transfer process between Bi^{3+} and Cr^{3+} in $Ca_3Ga_2Ge_3O_{12}$ host. As shown in Fig. 9, the slope of the straight line is $-\theta/3 = -1.93$ based on the PL data of this series of $Ca_3Ga_{1.94-x}Ge_3O_{12}$:$0.06Cr^{3+}$,$xBi^{3+}$ samples. The value of θ can be calculated as 5.79, which is close to six, meaning that the dipole–dipole interaction is the dominant mechanism for the interaction of Bi^{3+} and Cr^{3+} in the $Ca_3Ga_2Ge_3O_{12}$ phosphors. Moreover, the critical distance of Bi^{3+} and Cr^{3+} is also an essential parameter if we consider the concentration-quenching effect in this system. We can approximately estimate the critical distance from the report of Blasse, the critical distance (R_c) can be calculated as follows[20]

$$R_c \approx 2\left(\frac{3V}{4\pi x_c N}\right)^{\frac{1}{3}} \quad (4)$$

here, x_c is the critical concentration (the total concentration of sensitizer ions of Bi^{3+} and activator ions of Cr^{3+}), and N is the number of chemical formula in the unit cell, V is a volume of the unit cell. x_c is about 0.36 from the total concentration of Cr^{3+} (the concentration of 0.06) and Bi^{3+} (the concentration of 0.3). For the $Ca_3Ga_2Ge_3O_{12}$ host, the crystallographic parameters are $V = 1841.05$ Å^3, $N = 2$. The critical transfer distance is determined to be 16.97 Å. In general, there are two main reasons for the resonant energy-transfer mechanism: one is exchange interaction and the other is multipolar interaction.[21] If the critical distance between sensitizer and activator are shorter than 4 Å, the exchange interaction is the dominate way of energy transfer. As shown in Eq. (4), the critical transfer distance (R_c) is determined to be 16.97 Å. This value is much longer than 4 Å, indicating the possibility of energy transfer via the multipolar interaction mechanism, viz, dipole–dipole interaction as mentioned above.

The thermal stability of phosphor is one of important parameters for the potential application. Figures 10(a) and (b) show the PL spectra excited at 453 nm of the selected $Ca_3Ga_{1.94}Ge_3O_{12}$:$0.06Cr^{3+}$ (a) and Ca_3 $Ga_{1.64}Ge_3O_{12}$:$0.06Cr^{3+}$, $0.3Bi^{3+}$ (b) phosphors at different measurement temperature. Typically, the emission peak shifts to red as the temperature increases. With rising temperature, the bond lengths between the luminescent center (e.g., Cr^{3+}) and its ligand ions increase, leading to the decreased crystal field strength. So, it will cause the split of degenerate excited state or ground state, which results in the decrease in the transition energy. The variations in the emission intensities as a function of temperature for the two samples are further given for comparison in Fig. 10(c). From the picture we can see that with the increase in temperature from 30°C to 250°C, the PL intensity of $Ca_3Ga_{1.94}Ge_3O_{12}$:$0.06Cr^{3+}$ is found to be 70% of the initial value. As a comparison, the PL intensity of Ca_3 $Ga_{1.64}Ge_3O_{12}$:$0.06Cr^{3+}$,$0.3Bi^{3+}$ phosphor increases from room temperature to 100°C, which means that thermal stability of Cr^{3+} emission can be improved via the codoping Bi^{3+}. Above 100°C, the temperature-dependent emission intensity decrease slowly showing better thermal quenching

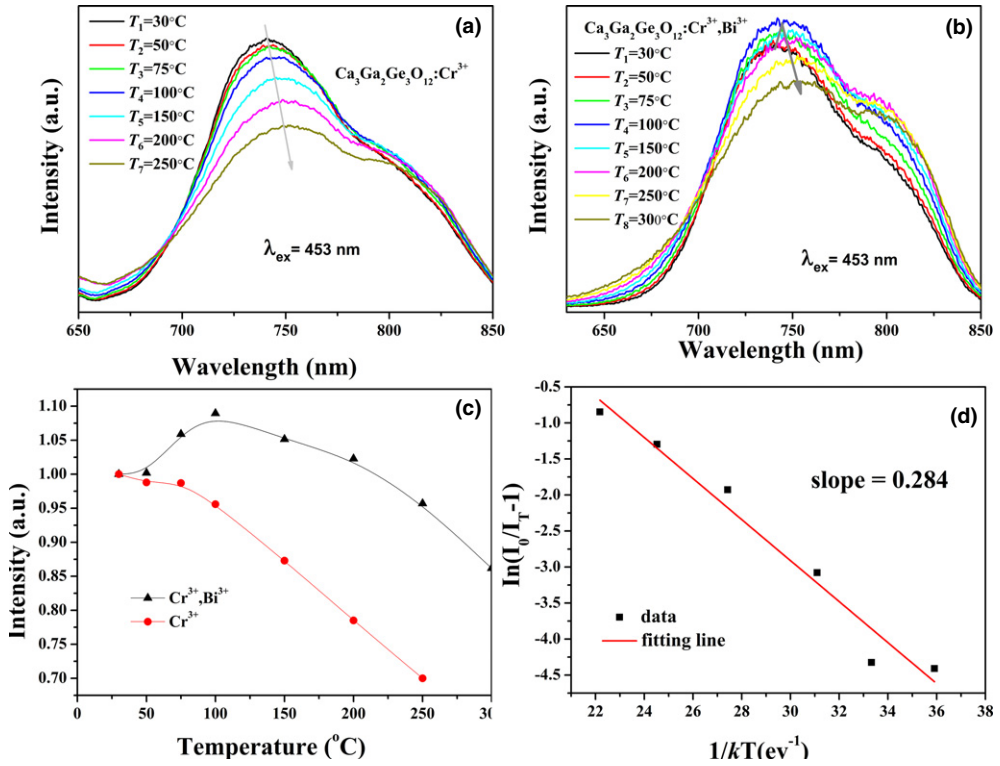

Fig. 10. The PL spectra (λ_{ex} = 453 nm) of $Ca_3Ga_{1.94}Ge_3O_{12}$:$0.06Cr^{3+}$ (a) and $Ca_3Ga_{1.94-x}Ge_3O_{12}$:$0.06Cr^{3+}$, $0.3Bi^{3+}$ (b) phosphors under different temperatures in the range of 30°C–300°C. (c) The variations in the emission intensities of $Ca_3Ga_{1.94}Ge_3O_{12}$:$0.06Cr^{3+}$ and $Ca_3Ga_{1.64}Ge_3O_{1.}$$0.06Cr^{3+}$, $0.3Bi^{3+}$ phosphors are given for comparison. (d) A $\ln[(I_0/I_T)-1]$ vs. $1/kT$ activation energy graph for thermal quenching of $Ca_3Ga_{1.94}Ge_3O_{12.}$$0.06Cr^{3+}$ phosphor.

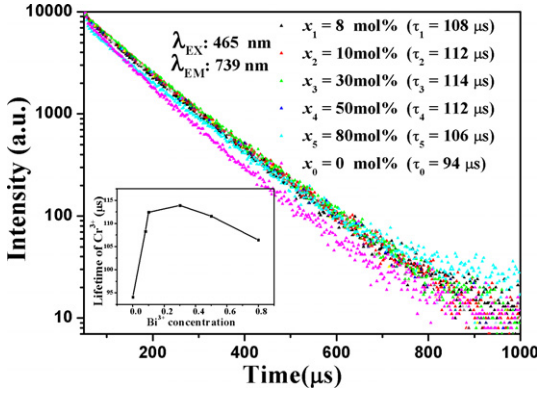

Fig. 11. Decay curves of Cr^{3+} emission at 739 nm in $Ca_3Ga_{1.94-x}Ge_3O_{12}$:0.06$Cr^{3+}$,$xBi^{3+}$ phosphors and the fitted lifetimes are also given in the figure.

properties than that of Cr^{3+} singly doped sample, such as similar temperature-dependent luminescence phenomenon has been previously studied.[22] To better understand the thermal quenching phenomena, the activation energy was fitted according to the Arrhenius equation[20,23]

$$I(T) = I_0/[1 + c\exp(-E/kT)] \quad (5)$$

where $I(T)$ is the PL intensity at different temperatures, I_0 is the initial PL intensity of the phosphor at 30°C, c is a constant, E is the activation energy for thermal quenching, and k is the Boltzmann constant(8.617×10^{-5} eV/K). As shown in Fig. 10(d), the plot of $\ln[(I_0/I_T)-1]$ vs. $1/kT$ yields a straight line, and the activation energy E for $Ca_3Ga_{1.94}Ge_3O_{12}$:0.06Cr^{3+} is obtained from the slope of the plot. According to the equation, we have obtained activation energy E to be 0.284 eV.

As the concentration of Cr^{3+} is fixed, and variation in lifetime value of Cr^{3+} dependent on Bi^{3+} content in $Ca_3Ga_{1.94}Ge_3O_{12}$:0.06Cr^{3+},xBi^{3+} phosphors is useful for the understanding of the energy-transfer process of Bi^{3+} and Cr^{3+} even if there are some impurities at high Bi^{3+} content. Figure 11 depicted the decay curves under excitation at 465 nm and monitored at 739 nm, corresponding to the $^2E \rightarrow {}^4A_2$ transition of Cr^{3+} for $Ca_3Ga_{1.94}Ge_3O_{12}$:0.06Cr^{3+}, xBi^{3+} phosphors, the fitted lifetimes were also given in the figure. All the decay curves can be well fitted with the first-order exponential decay mode.[24]

$$I(t) = A_1\exp(-t/\tau) \quad (6)$$

where I is the luminescence intensity at time t, and τ is the lifetime. A_1 is a constant. On the basis of Eq. (6) and the measured decay curves, the lifetime values were determined to be 94, 108, 112, 114, 112, and 106 μs for different Bi^{3+} concentrations of $x = 0$, 0.08, 0.10, 0.30, 0.50, and 0.80, respectively. As also given in the inset of Fig. 11, the lifetime values of the Cr^{3+} ions increased remarkably with increasing Bi^{3+} concentration and reaches the maximum value at Bi^{3+} concentration of 0.3. The increasing lifetime can prove the existence of energy transfer from the Bi^{3+} ions to Cr^{3+} ions. When the Bi^{3+} concentration was above 0.3, the lifetime values of the Cr^{3+} ions decreases, and it is believed to relate with the efficient energy transfer from Bi^{3+} to Cr^{3+}. The excessive Bi^{3+} content and appearance of impurity will quench the Cr^{3+} emission, so that the lifetime values decreased.

IV. Conclusions

In summary, $Ca_3Ga_2Ge_3O_{12}$:Cr^{3+} phosphors with NIR PL and LLP emission have been successfully developed. The crystal structure of $Ca_3Ga_2Ge_3O_{12}$ host was studied and determined based on the Rietveld refinements. Under excitation at 453 or 280 nm, $Ca_3Ga_2Ge_3O_{12}$:Cr^{3+} phosphors exhibit the broadband NIR emission peaking at 739 nm and the intensity of NIR emission can be enhanced owing to the ET behavior from Bi^{3+} to Cr^{3+} ions. The energy transfer from Bi^{3+} to Cr^{3+} in the $Ca_3Ga_2Ge_3O_{12}$ host has been demonstrated to be the dipole–dipole interaction, and the critical transfer distance is determined to be 16.97 Å. The thermally stable NIR luminescence properties can be also improved via the introduction of Bi^{3+}. The NIR LLP emission can be observed from the Cr^{3+}-doped $Ca_3Ga_2Ge_3O_{12}$ sample, and the introduction of Bi^{3+} can also enhance the afterglow properties, which made this series of phosphor be potential in the near future.

Acknowledgments

This work was supported by the National Natural Science Foundations of China (grant nos. 51002146, 51272242), Natural Science Foundations of Beijing (2132050), the Program for New Century Excellent Talents in University of Ministry of Education of China (NCET-12-0950), Beijing Nova Program (Z131103000413047), Beijing Youth Excellent Talent Program (YETP0635), the Funds of the State Key Laboratory of New Ceramics and Fine Processing, Tsinghua University (KF201306) and Fundamental Research Funds for the Central Universities (FRF-TP-14-005A1).

Supporting Information

Additional Supporting Information may be found in the online version of this article:

Data S1. The crystallographic information file (CIF) of $Ca_3Ga_2Ge_3O_{12}$ compound is given.

References

[1]T. Maldiney, G. Sraiki, B. Viana, D. Gourier, C. Richard, D. Scherman, M. Bessodes, K. Van den Eeckhout, D. Poelman, and P. F. Smet, "In Vivo Optical Imaging with Rare Earth Doped $Ca_2Si_5N_8$ Persistent Luminescence Nanoparticles," *Opt. Mater. Express*, **2**, 261–8 (2012).
[2]Y. Liu, D. Tu, H. Zhu, and X. Chen, "Lanthanide-Doped Luminescent Nanoprobes: Controlled Synthesis, Optical Spectroscopy and Bioapplications," *Chem. Soc. Rev.*, **42**, 6924–58 (2013).
[3]Z. W. Pan, Y. Y. Lu, and F. Liu, "Sunlight-Activated Long-Persistent Luminescence in the Near-Infrared from Cr^{3+}-Doped Zinc Gallogermanates," *Nat. Mater.*, **11**, 58–63 (2012).
[4]Y. X. Zhuang, J. Ueda, and S. Tanabe, "Tunable Trap Depth in Zn$(Ga_{1-x}Al_x)_2O_4$:Cr,Bi Red Persistent Phosphors: Considerations of High-Temperature Persistent Luminescence and Photostimulated Persistent Luminescence," *J. Mater. Chem. C*, **1**, 7849–55 (2013).
[5]B. Aurélie, J. Sylvaine, P. Kaustubh, L. Aurélie, V. Bruno, and G. Didier, "$ZnGa_2O_4$:Cr^{3+}: A New Red Long-Lasting Phosphor with High Brightness," *Opt. Express*, **19**, 10131–7 (2011).
[6]W. Z. Yan, F. Liu, Y. Y. Lu, X. J. Wang, M. Yin, and Z. W. Pan, "Near Infrared Long-Persistent Phosphorescence in $La_3Ga_5GeO_{14}$:Cr^{3+} Phosphor," *Opt. Express*, **18**, 20215–21 (2010).
[7]F. Liu, W. Z. Yan, Y. J. Chuang, Z. P. Zhen, J. Xie, and Z. W. Pan, "Photostimulated Near-Infrared Persistent Luminescence as a New Optical Read-Out from Cr^{3+}-Doped $LiGa_5O_8$," *Sci. Rep.*, **3**, 1554, 9pp (2013).
[8]A. Abdukayum, J. T. Chen, Q. Zhao, and X. P. Yan, "Functional Near Infrared-Emitting Cr^{3+}/Pr^{3+} Co-Doped Zinc Gallogermanate Persistent Luminescent Nanoparticles with Superlong Afterglow for *in Vivo* Targeted Bioimaging," *J. Am. Chem. Soc.*, **135**, 14125–33 (2013).
[9]S. K. Singh, "Red and Near Infrared Persistent Luminescence Nano-Probes for Bioimaging and Targeting Applications," *RSC Adv.*, **4**, 58674–98 (2014).
[10]S. Ye, J. J. Zhou, S. T. Wang, R. X. Hu, D. P. Wang, and J. R. Qiu, "Broadband Downshifting Luminescence in Cr^{3+}-Yb^{3+} Codoped Garnet for Efficient Photovoltaic Generation," *Opt. Express*, **21**, 4167–73 (2013).
[11]X. J. Zhou, L. Zhang, K. N. Zhou, Z. L. Wang, and Q. X. Li, "Generation of Broadband Emission by Incorporating N^{3-} into $Ca_3Sc_2Si_3O_{12}$:Ce^{3+} Garnet for High Rendering White LEDs," *J. Mater. Chem.*, **21**, 6354–8 (2011).
[12]D. Q. Chen, Y. Chen, H. W. Lu, and Z. G. Ji, "A Bifunctional Cr/Yb/Tm:$Ca_3Ga_2Ge_3O_{12}$ Phosphor with Near-Infrared Long-Lasting Phosphorescence and Upconversion Luminescence," *Inorg. Chem.*, **53**, 8638–45 (2014).
[13]Bruker AXS TOPAS V4: General Profile and Structure Analysis Software for Powder Diffraction Data–User's Manual, Bruker AXS, Karlsruhe, Germany (2008).
[14]P. D. Rack, J. J. Peterson, M. D. Potter, and W. Park, "Eu^{3+} and Cr^{3+} Doping for Red Cathodoluminescence in $ZnGa_2O_4$," *J. Mater. Res.*, **16**, 1429–33 (2001).

[15]M. Grinberg, "Spectroscopic Characterisation of Disordered Materials Doped with Chromium," *Opt. Matter*, **9**, 37–45 (2002).
[16]I. M. Peter, H. Brian, H. Keith, and G. Marek, "Substitutional Disorder and the Optical Spectroscopy of Gallogermanate Crystals," *J. Phys. Condens. Mater*, **8**, 3933–46 (1996).
[17]L. M. Chen, Y. M. Long, Y. M. Qin, and W. F. Li, "Co-Precipitation Preparation, Characterization and Optical Properties of Blue $CaSb_2O_6:Bi^{3+}$ Nano-Phosphor," *Mater. Lett.*, **102–103**, 59–61 (2013).
[18]G. Blasse, "Energy Transfer in Oxidic Phosphors," *Phys. Lett.*, **28**, 444–5 (1968).
[19]J. Zhou, Z. G. Xia, M. X. Yang, and K. Shen, "High Efficiency Blue-Emitting Phosphor: Ce^{3+}-Doped $Ca_{5.45}Li_{3.55}(SiO_4)_3O_{0.45}F_{1.55}$ for Near UV-Pumped Light-Emitting Diodes," *J. Mater. Chem.*, **22**, 21935–41 (2012).
[20]Z. G. Xia, R. S. Liu, K. W. Huang, and V. Drozd, "$Ca_2Al_3O_6F:Eu^{2+}$: A Green-Emitting Oxyfluoride Phosphor for White Light-Emitting Diodes," *J. Mater. Chem.*, **22**, 15183–9 (2012).
[21]Z. G. Xia and R. S. Liu, "Tunable Blue-Green Color Emission and Energy Transfer of $Ca_2Al_3O_6F:Ce^{3+},Tb^{3+}$ Phosphors for Near-UV White LEDs," *J. Phys. Chem. C*, **116**, 15604–9 (2012).
[22]R. Reisfeld, E. Greenberg, R. Velapoldi, and B. J. Barnett, "Luminescence Quantum Efficiency of Gd and Tb in Borate Glasses and the Mechanism Energy Transfer Between Them," *Chem. Phys.*, **56**, 1698–705 (1972).
[23]T. C. Liu, B. M. Cheng, S. F. Hu, and R. S. Liu, "Highly Stable Red Oxynitride β-SiAlON:Pr^{3+} Phosphor for Light-Emitting Diodes," *Chem. Mater.*, **23**, 3698–705 (2011).
[24]V. Bachmann, C. Ronda, and A. Meijerink, "Temperature Quenching of Yellow Ce^{3+} Luminescence in YAG:Ce," *Chem. Mater.*, **21**, 316–25 (2009). □